Microrheology reveals microscale viscosity gradients in planktonic systems

Òscar Guadayol[a,1], Tania Mendonca[b], Mariona Segura-Noguera[a], Amanda J. Wright[b], Manlio Tassieri[c], and Stuart Humphries[a]

[a]Joseph Banks Laboratories, School of Life Sciences, University of Lincoln, LN6 7DL Lincoln, United Kingdom; [b]Optics and Photonics Research Group, Department of Electrical and Electronic Engineering, University of Nottingham, NG7 2RD Nottingham, United Kingdom; and [c]Division of Biomedical Engineering, James Watt School of Engineering, University of Glasgow, G12 8LT Glasgow, United Kingdom

Edited by Tom M. Fenchel, University of Copenhagen, Helsingor, Denmark, and approved November 23, 2020 (received for review June 3, 2020)

Microbial activity in planktonic systems creates a dynamic and heterogeneous microscale seascape that harbors a diverse community of microorganisms and ecological interactions of global significance. In recent decades great effort has been put into understanding this complex system, particularly focusing on the role of chemical patchiness, while overlooking a physical parameter that governs microbial life and is affected by biological activity: viscosity. Here we reveal spatial heterogeneity of viscosity in planktonic systems by using microrheological techniques that allow measurement of viscosity at length scales relevant to microorganisms. We show the viscous nature and the spatial extent of the phycosphere, the region surrounding phytoplankton. In ∼45% of the phytoplankton cells analyzed we detected increases in viscosity that extended up to 30 μm away from the cell with up to 40 times the viscosity of seawater. We also show how these gradients of viscosity can be amplified around a lysing phytoplankton cell as its viscous contents leak away. Finally, we report conservative estimates of viscosity inside marine aggregates, hotspots of microbial activity, more than an order of magnitude higher than in seawater. Since the diffusivities of dissolved molecules, particles, and microorganisms are inversely related to viscosity, microheterogeneity in viscosity alters the microscale distribution of microorganisms and their resources, with pervasive implications for the functioning of the planktonic ecosystem. Increasing viscosities impacts ecological interactions and processes, such as nutrient uptake, chemotaxis, and particle encounter, that occur at the microscale but influence carbon and nutrient cycles at a global scale.

microscale patchiness | phytoplankton | extracellular polymeric substances | viscosity | passive microrheology

Planktonic microorganisms inhabit microenvironments far more complex and dynamic than suspected even two decades ago (1). Microbial activity, advection, and diffusive transport together create a patchy chemical landscape that within a few microliters sustains a diverse community of microalgae, protists, bacteria, and viruses, along with an intricate network of individual interactions and ecological processes of global significance (2–5). However, viscosity, a dominant feature of microbial life, has been overlooked in this emerging paradigm of microscale heterogeneity. Viscous forces govern directed motion and diffusion of microorganisms, particles, and molecules in the very low Reynolds numbers regime experienced by microbes. This implies that small microorganisms do not directly experience turbulent flows (6), that biomechanical plans that work for large organisms become inefficient for microbes (7), and that mass transfer is ultimately governed by molecular diffusivity (8), which is inversely proportional to viscosity. Several studies (compiled in ref. 9) have reported increases, often higher than one order of magnitude, of the bulk-phase viscosity of the water due to the presence in solution of extracellular polymeric substances (EPS) exuded by phytoplankton and bacteria (10). Moreover, it is known that intracellular viscosities can be up to two orders of magnitude higher than those in water (11). However, very little is known about the role viscosity plays in shaping the heterogeneous microscale landscape.

Here, we hypothesize the existence of microscale viscosity gradients created by the same biological processes that generate chemical gradients around planktonic microorganisms (3, 5). We argue that the existence of microscale patchiness in viscosity has fundamental implications for the distribution of microorganisms––and their resources—and therefore for the functioning of microbial planktonic ecosystems driving aquatic productivity globally.

To test our hypothesis, we characterized the variability in viscosity near microorganisms, nondestructively and at micrometer-length scales, by employing two methodologies from the fast-evolving field of microrheology: microrheology with optical tweezers (MOT) and multiple particle tracking microrheology (MPTM). We investigated three distinct scenarios where we expected viscosity to be heterogeneous: 1) the phycosphere around healthy EPS-exuding phytoplankton cells (5); 2) lysis events involving the release of cell contents; and 3) algal cell aggregates.

Results and Discussion

To test our hypothesis, we first took advantage of the high spatiotemporal resolution of MOT to measure viscosity near glass shards, as an inert control that mimics siliceous frustules, and near cells of *Chaetoceros affinis,* a diatom known to produce EPS

Significance

At the microscopic scales at which the life of marine microbes unfolds, the physics is dominated by viscosity. Increasing viscosity slows down both the passive transport of solutes and particles and the swimming of motile microorganisms, and thus directly or indirectly affects all aspects of microbial life. Viscosity depends not only on the physical properties of water, but it also varies as a consequence of biological activity, allowing microorganisms some control over their physical landscape. Our use of microrheology allows us to explore how viscosity is structured around phytoplankton cells and marine aggregates and unveils a level of spatial heterogeneity that has implications for the functioning of the microbial food web and hence of marine biogeochemical cycles.

Author contributions: Ò.G. and S.H. designed research; Ò.G., T.M., and M.S.-N. performed research; Ò.G., T.M., A.J.W., and M.T. contributed new analytic tools; Ò.G. and T.M. analyzed data; and Ò.G., T.M., M.S.-N., A.J.W., M.T., and S.H. wrote the paper.

The authors declare no competing interest.

This article is a PNAS Direct Submission.

[1]To whom correspondence may be addressed. Email: oscar@guadayol.cat.

This article contains supporting information online at https://www.pnas.org/lookup/suppl/doi:10.1073/pnas.2011389118/-/DCSupplemental.

Published December 21, 2020.

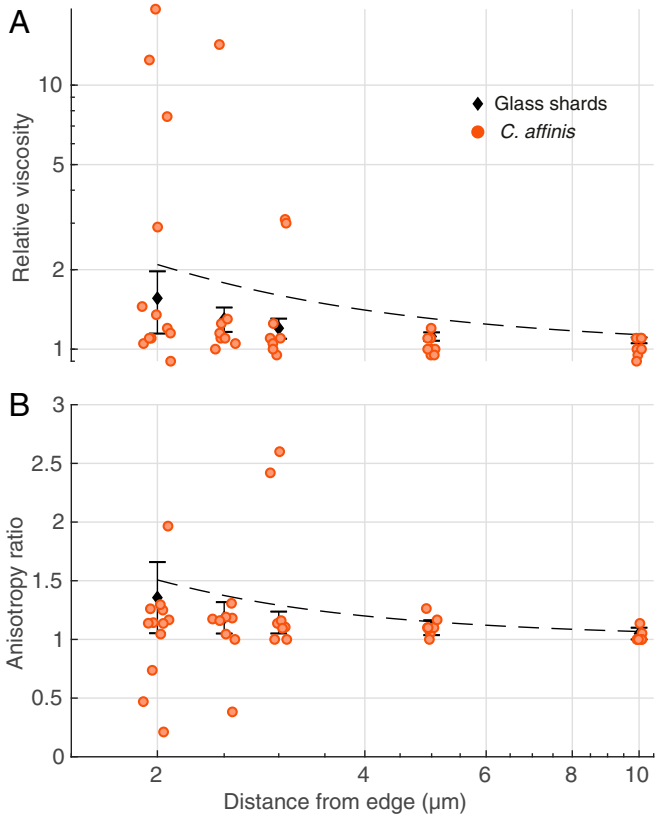

Fig. 1. MOT measurements of relative viscosity against distance from the boundary of the objects (phytoplankton cells or glass shards). Orange dots are individual measurements around *C. affinis* cells. Black diamonds are average ± SD of measurements around glass shards. Dashed black lines represent predictions from Faxén's laws (*Materials and Methods*). (*A*) Relative viscosity in the direction perpendicular to the edge of the object. (*B*) Anisotropy in the measurements, given as the ratio of relative viscosities in the perpendicular direction to those in the parallel direction. A value of 1 represents isotropy. Data have been jittered in the *x* direction by 0.1 μm to facilitate visualization.

and mucilages that lead to the formation of transparent exopolymer particles (TEP) (12, 13). Our results reveal that the relative viscosity (defined as the ratio of local dynamic viscosity to the dynamic viscosity of artificial seawater) is on average ∼2.6 times higher (along both axes analyzed; parallel to and approaching the edge of the cell or glass shard), and more variable near (at one probe-diameter's distance from) the cell wall of diatoms than near the glass shards (Fig. 1*A*). In the case of the diatoms, the relative viscosity is on average ∼2.2 times higher than predictions by Faxén's law (mean along both axes), which accounts for hydrodynamic interactions of a sphere near a solid wall (Fig. 1*A* and see also *Materials and Methods*). Moreover, for viscosity measurements taken near the diatoms, we also detected anisotropy in the observations recorded along the axes perpendicular and parallel to the cell wall (Fig. 1*B*), suggesting that EPS might be discretely patterned in space. These observations are consistent with studies showing the presence of mucilaginous or gel-like structures around fixed bacteria and phytoplankton exuding EPS (14–17) (*SI Appendix*, *Discussion*).

We next used MPTM to corroborate the MOT observations, maximize the spatial coverage of the rheological measurements, and investigate different species and scenarios. Maps of relative viscosity were generated around phytoplankton cells and within aggregates, with a field of view (FoV) of 130 × 175 μm^2 and a spatial resolution of 2 μm. The MPTM results for healthy *C. affinis* cells (Fig. 2 and *SI Appendix*, Fig. S1) are in good agreement with those obtained from MOT. In 30 of the 41 *C. affinis* cells analyzed, relative viscosities near the cell wall were statistically significantly higher than those predicted by Faxén's law. However, we did not observe any statistically significant increases in viscosity around glass shards (Fig. 3 and *SI Appendix*, Fig. S2, ref. 18), confirming that the high values recorded near the cells are not caused by hydrodynamic wall effects alone. As with MOT, relative viscosity values showed a tendency to decay nonlinearly away from the cell walls, suggesting exudation, diffusion, and clustering of EPS from the cell. In all explored cases, relative viscosities measured around *C. affinis* cells were highly variable, with areas showing enhanced values and others showing no notable increase. The extent of the viscous gradient around cells was also variable, ranging from 2 to more than 30 μm (Fig. 3).

To assess the prevalence of these viscous phycospheres, which we call "viscospheres," we next performed MPTM experiments on the diatoms *Cylindrotheca fusiformis* and *Skeletonema pseudocostatum*, on the dinoflagellates *Alexandrium minutum* and *Ostreopsis* cf. *ovata*, and on colonies of *Phaeocystis globosa*, a haptophyte whose blooms are often associated with submesoscale (∼1 km) increases in bulk-phase viscosity (19). We detected viscosity gradients around 45% of all cells analyzed, and in all species except for *C. fusiformis*. The presence of a viscous phycosphere or its spatial extent, contrary to our expectations based on diffusive rates (5), did not correlate with cell size, while there was a high degree of intra- and interspecific variability (Fig. 3). The spatial extent of the viscosphere for the entire dataset appeared to be negatively exponentially distributed (*SI Appendix*, Fig. S3), with large viscospheres being less frequent than small ones. Coefficients of variance of the two-dimensional (2D) viscosity maps ranged from 8 to >2,000 in all MPTM experiments

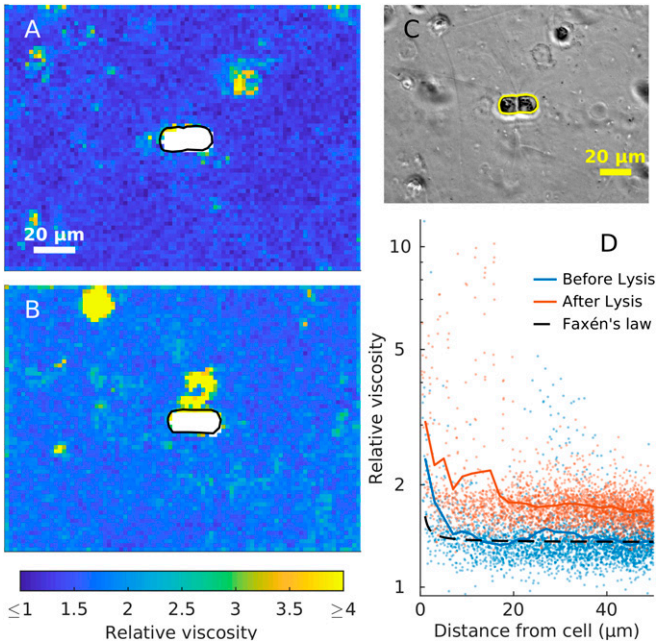

Fig. 2. Viscosity changes around a *C. affinis* cell (*A*) before and (*B*) 1 h after light-induced cell lysis. (*A* and *B*) 2 × 2 μm MPTM viscosity maps. (*C*) Phase-contrast image at the start of the experiment. Cell boundaries are drawn in black in *A* and *B*, and yellow in *C*. (*D*) Viscosity estimates against the minimum distance to the boundary of the cell before (blue) and after (red) the lysis. Colored lines are a moving average with a 2-μm window. Dashed black line represents Faxén's law for motion perpendicular to a solid boundary (Eq. **2**).

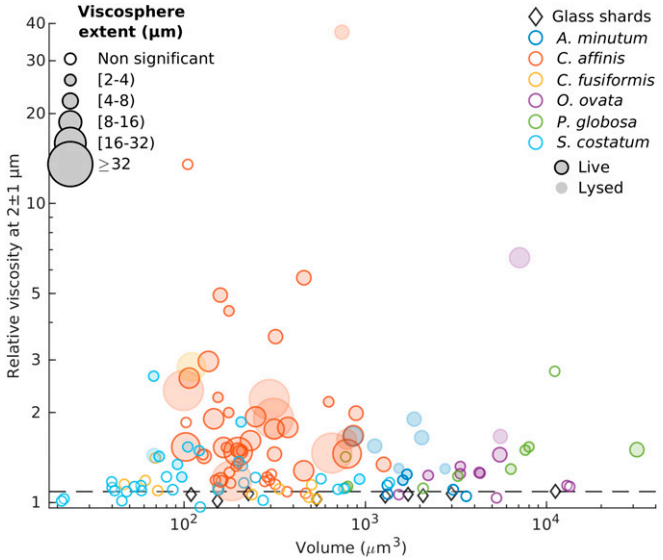

Fig. 3. Average relative viscosities between 1 and 3 μm away from cells in relation to cells volume. The diameter of each symbol is proportional to the extent of the viscous phycosphere. Horizontal dashed line represents predictions from Faxén's law for motion perpendicular to a solid boundary (Eq. **2**).

(*SI Appendix*, Table S1), suggesting that viscous patches are not only associated with cells and can also mark the presence of colloids and mucus sheets (2). The highest relative viscosity values we recorded (up to 80) were found inside the mucopolysaccharide matrix of *P. globosa* colonies (*SI Appendix*, Fig. S4).

The existence of a viscosphere around phytoplankton cells has profound implications beyond the physiological and ecological roles so far attributed to EPS (20, 21) as it fundamentally reshapes the cells' physical environment. Exopolymers allow microalgae to structure the phycosphere and modify flow fields (22). Critically, and although the diffusivity of small molecules depends on a number of factors and cannot be quantified with our viscosity data (*SI Appendix*, *Discussion*), an increase in viscosity reduces molecular diffusivities, slowing nutrient uptake, waste removal, and exchange of infochemicals. It may also influence bacterial distributions around microalgae, not only because lower molecular diffusivities lead to steeper, longer-lived, and easier to track gradients of chemoattractants, but also because viscosity affects the swimming speed of bacteria (23) and therefore their distribution. Although responses to viscosity are species-specific and dome-shaped, in most cases microorganisms slow down at high viscosities (24, 25). Thus, a gradient in viscosity around a phytoplankton cell will translate into a gradient of bacterial motility, which has been shown to lead to accumulation of bacteria (26). Consequently, we propose EPS exudation as an active strategy to recruit symbiotic bacteria to the phycosphere (*SI Appendix*, *Discussion*).

Viscosity gradients are also expected to develop when cells lyse, as intracellular viscosities can be several orders of magnitude higher than water (11). To test this hypothesis, we used MPTM to map viscosity around *C. affinis* cells before and after light-induced lysis (27), as well as around dead *S. pseudocostatum*, *A. minutum,* and *O. ovata* cells. We detected statistically significant increases in background viscosities of between 4 and 29% after exposure to UV and bright light in eight out of nine *C. affinis* samples, most likely because all cells within the FoV were lysed. Additionally, we observed localized and persistent patches of high viscosity around lysed cells (Fig. 2), as well as steep viscosity gradients around dead cells. Lysing and dead cells are hotspots of microbial activity, as chemotactic bacteria swarm around them (27). Therefore, we expect the same mechanisms at play in a viscous phycosphere to be magnified in a lysing cell, leading to a more efficient use of resources by chemotactic bacteria.

The last scenario we explored was of viscosity gradients generated by aggregates of phytoplankton. The formation of aggregates, TEP, and marine snow is facilitated by EPS acting as a loose adhesive (12). We used MPTM to map relative viscosities inside and around shear-induced aggregates of the three diatom cultures. We observed increases in viscosity of more than one order of magnitude inside the aggregates (Fig. 4), with areas of enhanced viscosity largely overlapping areas stained by Calcofluor white (specific for β-d-glucopyranose polysaccharides). We regard these estimates as conservative because the spatial coverage of the MPTM maps inside the aggregates is limited by the capacity of the microspheres to penetrate the aggregates and by self-shading. Nonetheless, given the important role that aggregates play as hotspots for zooplankton foraging and microbial activity and the importance of diffusive processes in sinking of porous particles in stratified water columns (28), we believe maps of viscosity such as those we present here will allow a more accurate characterization of processes influencing the biological carbon pump, such as the flux of chemicals that controls remineralization rates inside the aggregates (29) and the sinking speed of marine snow.

The implications of microscale viscosity gradients are grounded in fundamental physics and are pervasive, as viscosity impacts virtually all processes and interactions occurring in the microbial world. A quantitative assessment of these implications is still not possible, given current knowledge on the functional responses of relevant processes to viscosity (*SI Appendix*, *Discussion* for an in-depth treatment of this topic). However, we can be certain that increasing viscosity decreases the diffusivity of dissolved substances, small passive particles, and organisms, and slows motile plankton and sinking particles. Therefore, changes in viscosity not only affect the distribution of organisms and their resources, but also slow ecological rates, resulting in a cascade of effects at different ecological levels and scales (*SI Appendix*, *Discussion*). Increasing viscosity around osmotrophs decreases nutrient uptake rates, impacting primary and bacterial productivities. Similar reductions in encounter rates between predators (or viruses) and prey (or hosts), along with uncertain effects on the formation and sedimentation of aggregates, ultimately influence the transfer of carbon across trophic levels and the strength of the biological carbon pump. In summary, the inclusion of viscosity adds a layer of complexity to the current paradigm of microscale heterogeneity. The use of microrheological techniques, capable of delivering maps of viscosity with spatial resolution relevant to microorganisms, will allow a quantitative exploration of how these ideas unfold from the microscale upwards.

Materials and Methods

Phytoplankton Species and Cultures: Formation of Aggregates.
Growth conditions. We performed our experiments on the diatoms *C. affinis* (CCAP 1010/27), *C. fusiformis* (CCAP 1017/2), and *S. pseudocostatum* (CCAP 1077/7), the dinoflagellates *A. minutum* (CCAP 1119/15), and *O. ovata* (OOPM17), and the haptophyte *P. globosa* (strains K-1321 and K-1323, Norwegian Culture Collection of Algae). Diatoms were grown in f/2 + Si medium (30) in 33.5 g/L artificial seawater (ASW, Aquarium Systems Instant Ocean Salt). *A. minutum* and *P. globosa* K-1323 were grown on L1 medium (31) in 30 g/L ASW. *P. globosa* K-1321 was grown on TL medium (Norwegian Culture Collection of Algae) in 30 g/L ASW. All species, except *O. ovata*, were grown at 19 °C without shaking in an algae incubator (Algaetron AG 230, Photon Systems Instruments) with a 12:12-h illumination cycle. The light intensity was 100 μE for diatoms and 90 μE for *A. minutum* and *P. globosa*. *O. ovata* was grown with L1 medium in 38.5 g/L ASW and kept at laboratory temperature (20 °C) on a windowsill to ensure it received enough illumination. *C. affinis* cultures for the MOT experiments were also grown at room

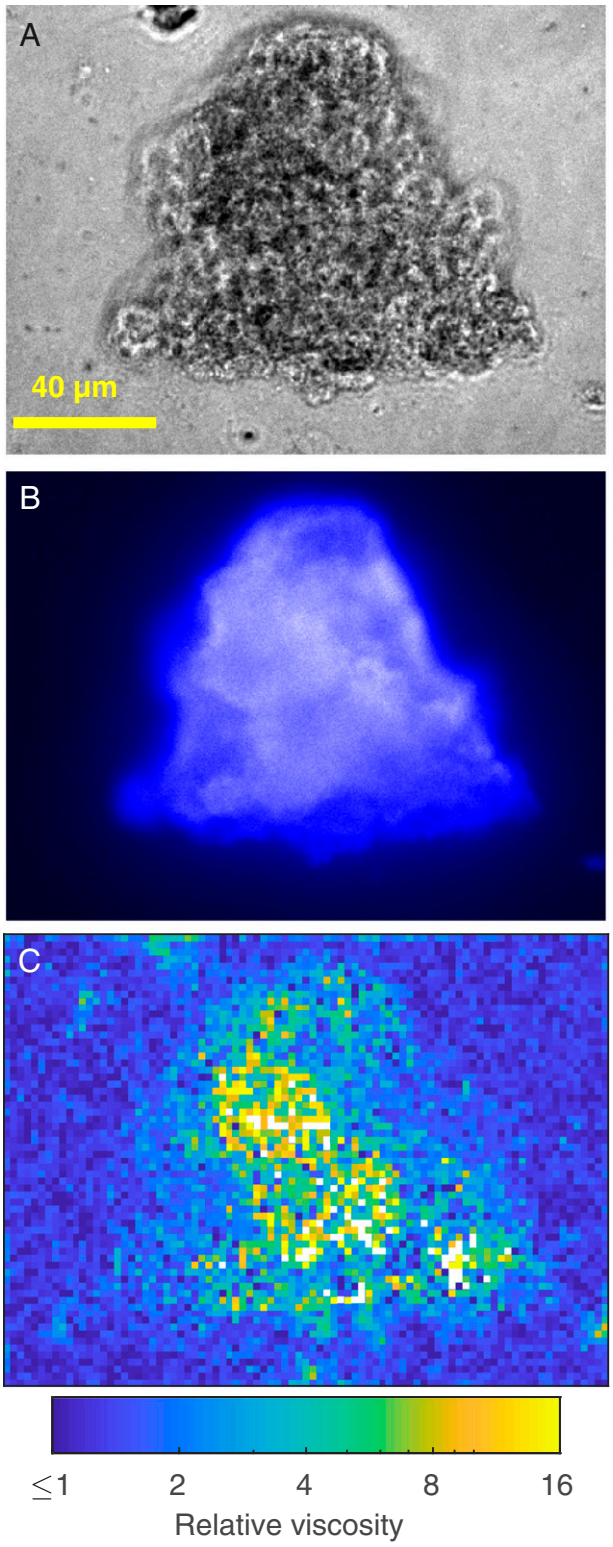

Fig. 4. Viscosity measurements inside and around a *C. affinis* aggregate. (*A*) Phase-contrast image. (*B*) CFW staining for polysaccharides. (*C*) Viscosity map with 2 × 2 μm binning obtained with MPTM. White pixels are areas with too few microsphere tracks to provide a reliable estimate.

temperature on a windowsill. Since cultures were not axenic, to ensure few bacteria were present during the experiments, these were carried out less than 2 wk after media refreshment.

Aggregates of cells were formed from *C. affinis*, *C. fusiformis*, and *S. pseudocostatum* cultures by incubating newly refreshed monocultures on a roller table (32). The roller was on the windowsill with natural light conditions at 20 °C. Within a few hours, aggregates were visible. Individual aggregates were collected very gently with a capillary tube to restrict disruption and prepared for MPTM analysis using the same protocol as for phytoplankton below.

MOT. We performed MOT to measure viscosity around *C. affinis* and around inert glass shards that mimicked the siliceous frustule of a diatom. MOT uses single, optically trapped microspheres as probes for measuring the rheological properties of the material surrounding them. Each microsphere is held by a tightly focused laser beam and can be manipulated in three-dimensional space, allowing it to be placed at specific locations around an object of interest (e.g., a phytoplankton cell). A microsphere confined within an optical trap will move with amplitudes on the nanometer scale due to the thermal fluctuations of the molecules of the surrounding material. The time-dependent mean-squared displacement calculated from the residual motion of a trapped microsphere can be used to compute the rheological properties of the fluid around it as well as the strength of the optical trap (33–36). The relative viscosity (defined as the ratio of local absolute viscosity to that of ASW) around *C. affinis* cells and glass shards was calculated by plotting the microsphere's normalized position autocorrelation function against time (34). Details on our use of MOT are given in *SI Appendix, Materials and Methods*.

Edge effects. In all our calculations we accounted for the hydrodynamic effects caused by the proximity to a solid object. A moving sphere experiences an increase in hydrodynamic drag at close proximity to a solid surface. Since the hydrodynamic drag coefficient γ is proportional to the dynamic viscosity η of the fluid, this effect translates into an apparent increase in the viscosity of the fluid near the boundary. This increase in γ has been estimated by Faxén's law (37, 38) and depends on the radius of the sphere *a*, its distance from the surface *s*, and the viscosity of the material in which the sphere is suspended. Faxén's effect experienced by a microsphere moving parallel to the surface is given by (39)

$$\gamma^{\parallel} = \frac{\gamma}{1-(9/16)(a/s)+(1/8)(a/s)^3}, \quad [1]$$

where $\gamma^{\parallel}$ is the corrected hydrodynamic drag coefficient for a sphere moving parallel to the surface, γ is the hydrodynamic drag coefficient far from the surface, which for a sphere is $\gamma = 6\ \pi\ a\ \eta$. Similarly, for the microsphere's motion perpendicular to the surface Faxén's effect is

$$\gamma^{\perp} = \frac{\gamma}{1-(9/8)(a/s)+(1/2)(a/s)^3}, \quad [2]$$

where $\gamma^{\perp}$ is the corrected hydrodynamic drag coefficient for a sphere moving perpendicular to the surface. The apparent increase in relative viscosity due purely to hydrodynamic effects close to a boundary wall, in the parallel and perpendicular directions, is given by the ratio of the drag coefficients $\gamma^{\parallel}/\gamma$ and $\gamma^{\perp}/\gamma$, respectively.

Anisotropy. We assessed the anisotropy of the local relative viscosity measured using MOT by calculating the ratio of the relative viscosity measured from the particle motion perpendicular to the edge of the cell or glass shard by the relative viscosity measured from the particle motion parallel to the edge of the cell or glass shard. Fig. 1*B* includes Faxén's effect and hence the effects purely due to the hydrodynamics near a solid wall by plotting $\gamma^{\perp}/\gamma^{\parallel}$ for varying distances from the edge of the object.

Passive MPTM. To assess spatial variability in viscosity at the microscale, we used passive MPTM (40). Briefly, the sample of interest was seeded with fluorescent microspheres of known diameter and density. The microspheres were tracked under the microscope as they underwent free Brownian motion. From analyses of their trajectories, and given a known and constant temperature, it is possible to estimate the local dynamic viscosity of the fluid into which the microspheres were suspended. We partitioned the 2D field of view into squares of given length and estimated average dynamic viscosity from analysis of all tracks registered within each square. This procedure allowed us to generate maps of relative viscosity with a resolution of 2 μm, around individual phytoplankton cells as well as around, and to a certain extent within, aggregates. All our maps have been published without any preselection in a Figshare collection (18). Details on the sample preparation and visualization and the calculation of viscosity are given in *SI Appendix, Materials and Methods*

Lysis of individual phytoplankton cells was induced by exposing them to ultraviolet (UV) and white light at maximum intensity for ~10 min, following Smriga et al. (27). The field of illumination was narrowed to minimize effects on nearby cells. In the case of diatoms, the lysing procedure was deemed successful when motile bacteria started to aggregate around the cell (signaling release of material). To avoid hydrodynamic interactions of swimming bacteria with the microspheres, we waited until the cloud of bacteria had dissipated before starting the recordings, which could take at least 10 min but no more than 1 h. In the case of dinoflagellates, which are motile, we immobilized the cells by exposing them to UV and white light at the maximum intensity for a short period. Upon exposure to intense light *A. minutum* cells would first lose the lateral flagellum and then the polar one. If the light were left on longer, a "blob" of material would be seen coming out of the cell.

Exopolymer staining. Simultaneously with the MPTM of aggregates we assayed staining of the sample with several labels commonly used to visualize different EPS components in biofilms and flocs (41, 42). Explicitly, we tested 1) Alcian blue (Sigma-Aldrich A5268), which is specific for negatively charged polysaccharides commonly used to dye transparent exopolymer particles (43), 2) FilmTrace SYPRO Ruby (Thermo Fisher Scientific F10318), which labels most proteins, 3) SYBR Green I, which labels nucleic acids, 4) Con A-Tetramethylrhodamine conjugate (Con A, Invitrogen C860), which labels α-d-Glucose and α-d-mannose and 5) Calcofluor white M2R (CFW, Sigma-Aldrich 18909), which labels β-d-glucopyranose polysaccharides. Alcian blue revealed an intricate network of polysaccharides within our samples, but we did not use it alongside MPTM because it precipitates in the presence of salts, creating a rigid matrix that alters the rheological properties of the fluid. Of the other stains, Con A and CFW produced the highest signal. In subsequent analyses of aggregates we used CFW.

Data Availability. A collection of viscosity maps and figure data has been deposited in Figshare (https://doi.org/10.6084/m9.figshare.c.4534553.v3).

ACKNOWLEDGMENTS. We thank E. Berdalet, F. el Baidouri, R. Holzman, C. Marrasé, F. Peters, R. Schuech, and R. Simó for comments on previous versions of this manuscript. We thank E. Berdalet for providing *O. ovata* and S. Vaidyanathan for providing *C. fusiformis*. This work was funded by a Gordon and Betty Moore Foundation Marine Microbiology Initiative award, Grant 6852 (to S.H. and Ò.G). M.T., A.J.W., and T.M. acknowledge support through Engineering and Physical Sciences Research Council/Biotechnology and Biological Sciences Research Council/Medical Research Council Grants (EP/R035067/1, EP/R035563/1, and EP/R035156/1).

1. F. Azam, Microbial control of oceanic carbon flux: The plot thickens. *Science* **280**, 694–696 (1998).
2. F. Azam, F. Malfatti, Microbial structuring of marine ecosystems. *Nat. Rev. Microbiol.* **5**, 782–791 (2007).
3. R. Stocker, Marine microbes see a sea of gradients. *Science* **338**, 628–633 (2012).
4. M. A. Moran, The global ocean microbiome. *Science* **350**, aac8455 (2015).
5. J. R. Seymour, S. A. Amin, J.-B. Raina, R. Stocker, Zooming in on the phycosphere: The ecological interface for phytoplankton-bacteria relationships. *Nat. Microbiol.* **2**, 17065 (2017).
6. F. Peters, C. Marrasé, Effects of turbulence on plankton: An overview of experimental evidence and some theoretical considerations. *Mar. Ecol. Prog. Ser.* **205**, 291–306 (2000).
7. R. Schuech, T. Hoehfurtner, D. J. Smith, S. Humphries, Motile curved bacteria are pareto-optimal. *Proc. Natl. Acad. Sci. U.S.A.* **116**, 14440–14447 (2019).
8. L. Karp-Boss, E. Boss, P. A. Jumars, Nutrient fluxes to planktonic osmotrophs in the presence of fluid motion. *Oceanogr. Mar. Biol. Annu. Rev.* **34**, 71–107 (1996).
9. I. R. Jenkinson, J. Sun, Rheological properties of natural waters with regard to plankton thin layers. A short review. *J. Mar. Syst.* **83**, 287–297 (2010).
10. I. R. Jenkinson, X. X. Sun, L. Seuront, Thalassorheology, organic matter and plankton: Towards a more viscous approach in plankton ecology. *J. Plankton Res.* **37**, 1100–1109 (2015).
11. D. Wirtz, Particle-tracking microrheology of living cells: Principles and applications. *Annu. Rev. Biophys.* **38**, 301–326 (2009).
12. T. Kiørboe, J. L. S. Hansen, Phytoplankton aggregate formation: Observations of patterns and mechanisms of cell sticking and the significance of exopolymeric material. *J. Plankton Res.* **15**, 993–1018 (1993).
13. S. Myklestad, O. Holm-Hansen, K. M. Vårum, B. E. Volcani, Rate of release of extracellular amino acids and carbohydrates from the marine diatom *Chaetoceros affinis*. *J. Plankton Res.* **11**, 763–773 (1989).
14. F. Malfatti, F. Azam, Atomic force microscopy reveals microscale networks and possible symbioses among pelagic marine bacteria. *Aquat. Microb. Ecol.* **58**, 1–14 (2009).
15. G. Pletikapić *et al*., AFM imaging of extracellular polymer release by marine diatom *Cylindrotheca closterium* (Ehrenberg) Reiman & J.C. Lewin. *J. Mol. Recognit.* **24**, 436–445 (2011).
16. E.-M. Zetsche, A. El Mallahi, F. J. R. Meysman, Digital holographic microscopy: A novel tool to study the morphology, physiology and ecology of diatoms. *Diatom Res.* **31**, 1–16 (2016).
17. K. Li *et al*., Capsular polysaccharide production from *Zunongwangia profunda* SM-A87 monitored at single cell level by atomic force microscopy. *Deep Sea Res. Part II* **155**, 44–49 (2018).
18. Ò. Guadayol, M. Segura Noguera, S. Humphries, A collection of 2-D viscosity maps around phytoplankton cells and aggregates. *Figshare*. https://doi.org/10.6084/m9.figshare.c.4534553.v3. Deposited 12 November 2020.
19. L. Seuront, D. Vincent, J. G. Mitchell, Biologically induced modification of seawater viscosity in the Eastern English Channel during a *Phaeocystis globosa* spring bloom. *J. Mar. Syst.* **61**, 118–133 (2006).
20. C. S. Reynolds, Variability in the provision and function of mucilage in phytoplankton: Facultative responses to the environment. *Hydrobiologia* **578**, 37–45 (2007).
21. A. W. Decho, T. Gutierrez, Microbial extracellular polymeric substances (EPSs) in ocean systems. *Front. Microbiol.* **8**, 922 (2017).
22. T. Wyatt, M. R. d'Alcalà, "Dissolved organic matter and planktonic engineering" in *CIESM Workshop Monographs No. 28: Production and Fate of Dissolved Organic Matter in the Mediterranean Sea* (CIESM Publisher, Monaco, 2006), pp. 13–23.
23. V. A. Martinez *et al*., Flagellated bacterial motility in polymer solutions. *Proc. Natl. Acad. Sci. U.S.A.* **111**, 17771–17776 (2014).
24. S. Humphries, A physical explanation of the temperature dependence of physiological processes mediated by cilia and flagella. *Proc. Natl. Acad. Sci. U.S.A.* **110**, 14693–14698 (2013).
25. E. Lauga, Bacterial hydrodynamics. *Annu. Rev. Fluid Mech.* **48**, 105–130 (2016).
26. M. Demir, H. Salman, Bacterial thermotaxis by speed modulation. *Biophys. J.* **103**, 1683–1690 (2012).
27. S. Smriga, V. I. Fernandez, J. G. Mitchell, R. Stocker, Chemotaxis toward phytoplankton drives organic matter partitioning among marine bacteria. *Proc. Natl. Acad. Sci. U.S.A.* **113**, 1576–1581 (2016).
28. K. Kindler, A. Khalili, R. Stocker, Diffusion-limited retention of porous particles at density interfaces. *Proc. Natl. Acad. Sci. U.S.A.* **107**, 22163–22168 (2010).
29. N. Moradi *et al*., A new mathematical model to explore microbial processes and their constraints in phytoplankton colonies and sinking marine aggregates. *Sci. Adv.* **4**, eaat1991 (2018).
30. R. R. L. Guillard, J. H. Ryther, Studies of marine planktonic diatoms. I. Cyclotella nana Hustedt, and Detonula confervacea (cleve) Gran. *Can. J. Microbiol.* **8**, 229–239 (1962).
31. R. R. L. Guillard, P. E. Hargraves, *Stichochrysis immobilis* is a diatom, not a chrysophyte. *Phycologia* **32**, 234–236 (1993).
32. A. L. Shanks, E. W. Edmondson, Laboratory-made artificial marine snow: A biological model of the real thing. *Mar. Biol.* **101**, 463–470 (1989).
33. M. Tassieri, Microrheology with optical tweezers: Peaks & troughs. *Curr. Opin. Colloid Interface Sci.* **43**, 39–51 (2019).
34. M. Tassieri *et al*., Microrheology with optical tweezers: Measuring the relative viscosity of solutions 'at a glance'. *Sci. Rep.* **5**, 8831 (2015).
35. F. Watts *et al*., Investigating the micro-rheology of the vitreous humor using an optically trapped local probe. *J. Opt.* **16**, 015301 (2013).
36. A. Yao, M. Tassieri, M. Padgett, J. Cooper, Microrheology with optical tweezers. *Lab Chip* **9**, 2568–2575 (2009).
37. H. Faxén, Der Widerstand gegen die Bewegung einer starren Kugel in einer zähen Flüssigkeit, die zwischen zwei parallelen ebenen Wänden eingeschlossen ist. *Ann. Phys.* **373**, 89–119 (1922).
38. M. P. Lee, G. M. Gibson, D. Phillips, M. J. Padgett, M. Tassieri, Dynamic stereo microscopy for studying particle sedimentation. *Opt. Express* **22**, 4671–4677 (2014).
39. J. Leach *et al*., Comparison of Faxén's correction for a microsphere translating or rotating near a surface. *Phys. Rev. E Stat. Nonlin. Soft Matter Phys.* **79**, 026301 (2009).
40. E. M. Furst, T. M. Squires, *Microrheology* (Oxford University Press, Oxford, 2017), pp. 480.
41. B. S. McSwain, R. L. Irvine, M. Hausner, P. A. Wilderer, Composition and distribution of extracellular polymeric substances in aerobic flocs and granular sludge. *Appl. Environ. Microbiol.* **71**, 1051–1057 (2005).
42. M. Pan, L. Zhu, L. Chen, Y. Qiu, J. Wang, Detection techniques for extracellularpolymeric substances in biofilms: A review. *BioResources* **11**, 8092–8115 (2016).
43. A. L. Alldredge, M. W. Silver, Characteristics, dynamics and significance of marine snow. *Prog. Oceanogr.* **20**, 41–82 (1988).